Since January 2020 Elsevier has created a COVID-19 resource centre with free information in English and Mandarin on the novel coronavirus COVID-19. The COVID-19 resource centre is hosted on Elsevier Connect, the company's public news and information website.

Biochemical and Biophysical Research Communications 601 (2022) 129–136

Contents lists available at ScienceDirect

Biochemical and Biophysical Research Communications

journal homepage: www.elsevier.com/locate/ybbrc

The stalk domain of SARS-CoV-2 NSP13 is essential for its helicase activity

Kun Yue [a, b, 1], Bin Yao [a, b, 1], Yingchao Shi [a, b, 1], Yang Yang [a, b], Zhaohui Qian [c], Yali Ci [a, b, **], Lei Shi [a, b, *]

[a] State Key Laboratory of Medical Molecular Biology, Institute of Basic Medical Sciences, Chinese Academy of Medical Sciences and School of Basic Medicine, Peking Union Medical College, Beijing, 100005, China
[b] Department of Biochemistry and Molecular Biology, Institute of Basic Medical Sciences, Chinese Academy of Medical Sciences and School of Basic Medicine, Peking Union Medical College, Beijing, 100005, China
[c] Institute of Pathogen Biology, Chinese Academy of Medical Sciences, Beijing, 100176, China

ARTICLE INFO

Article history:
Received 17 February 2022
Accepted 18 February 2022
Available online 23 February 2022

Keywords:
SARS-CoV-2
NSP13
Helicase
Stalk
Rigid connection

ABSTRACT

COVID-19, caused by SARS-CoV-2, has been spreading worldwide for more than two years and has led to immense challenges to human health. Despite the great efforts that have been made, our understanding of SARS-CoV-2 is still limited. The viral helicase, NSP13 is an important enzyme involved in SARS-CoV-2 replication and transcription. Here we highlight the important role of the stalk domain in the enzymatic activity of NSP13. Without the stalk domain, NSP13 loses its dsRNA unwinding ability due to the lack of ATPase activity. The stalk domain of NSP13 also provides a rigid connection between the ZBD and helicase domain. We found that the tight connection between the stalk and helicase is necessary for NSP13-mediated dsRNA unwinding. When a short flexible linker was inserted between the stalk and helicase domains, the helicase activity of NSP13 was impaired, although its ATPase activity remained intact. Further study demonstrated that linker insertion between the stalk and helicase domains attenuated the RNA binding ability and affected the thermal stability of NSP13. In summary, our results suggest the crucial role of the stalk domain in NSP13 enzymatic activity and provide mechanistic insight into dsRNA unwinding by SARS-CoV-2 NSP13.

1. Introduction

The coronavirus disease 2019 (COVID-19) pandemic has changed the world in an unprecedently way, leading to more than 4 billion infections and 5 million deaths. It has been proclaimed a public health emergency by the WHO for two years. Currently, SARS-CoV-2 variants are constantly still spreading worldwide [1,2]. However, our understanding of SARS-CoV-2 remains limited. It is necessary to explore the mechanism of viral replication, to potentially provide new antiviral targets and strategies.

SARS-CoV-2 is a beta-coronavirus (CoV) belonging to the family Coronaviridae [3–5]. The other two CoVs that have caused serious threats in recent years are severe acute respiratory syndrome coronavirus (SARS-CoV, in 2003) [6,7]and Middle East respiratory syndrome coronavirus (MERS-CoV, in 2012) [8,9]. SARS-CoV-2 is an enveloped virus with a positive-sense single-stranded RNA genome of ~30 kb [10,11]. The SARS-CoV-2 genome encodes 16 nonstructural proteins (NSP1-16), four structural proteins (membrane (M), spike (S), envelope (E) and nucleocapsid (N)) and several accessory proteins (ORF3a, 3b, p6, 7a, 7b, 8b, 9b, and 14) [12,13].

SARS-CoV-2 NSP13 is a virus-encoded helicase that unwinds viral dsRNA intermediates to provide a single-stranded template for viral RNA amplification [14]. NSP13 of SARS-CoV-2 is highly conserved relative to that of SARS-CoV, with 99.8% protein sequence identity [15]. It is a member of the superfamily 1 (SF1) helicases, and has several conserved motifs and similar unwinding activity [16,17]. SARS-CoV or SARS-CoV-2 NSP13 unwinds dsDNA/dsRNA strands with a 5′ overhang in the 5′ to 3’ direction in a

* Corresponding author. State Key Laboratory of Medical Molecular Biology, Institute of Basic Medical Sciences, Chinese Academy of Medical Sciences and School of Basic Medicine, Peking Union Medical College, Beijing, 100005, China.
** Corresponding author. State Key Laboratory of Medical Molecular Biology, Institute of Basic Medical Sciences, Chinese Academy of Medical Sciences and School of Basic Medicine, Peking Union Medical College, Beijing, 100005, China.
E-mail addresses: ciyali@ibms.pumc.edu.cn (Y. Ci), shilei@ibms.pumc.edu.cn (L. Shi).
[1] These authors contribute equally to this work.

https://doi.org/10.1016/j.bbrc.2022.02.068
0006-291X/

manner dependent on ATP hydrolysis, without discrimination between dsRNA and dsDNA [18–21]. It is composed of an N-terminal zinc-binding domain (ZBD), a stalk domain and a helicase domain at the C-terminus [22]. The ZBD domain of SARS-CoV NSP13 has been shown to be necessary for its helicase activity [23]. However, the function and mechanism of the NSP13 stalk domain are still unclear.

Here we investigated the contribution of the stalk domain to the enzymatic activity of SARS-CoV-2 NSP13. We found that deletion of the stalk domain almost completely abolishes the ATPase activity of SARS-CoV-2 NSP13, indicating its essential role in NSP13 activity. Moreover, NSP13 helicase activity was also disrupted when we inserted a flexible linker between the stalk and helicase domains. Further investigation showed that insertion of the flexible linker affected the RNA binding but not the ATPase activity of NSP13. Linker insertion between the stalk and helicase domains also reduced the protein stability of NSP13. Collectively, these findings indicate that the stalk domain provides a rigid connection between the ZBD and helicase domain, contributing to the RNA binding and enzyme activity of NSP13.

2. Materials and methods

2.1. Clone construction

The SARS-CoV-2 NSP13 gene fragment was constructed into pET15b vector between *Nde*I and *Xho*I. D374A/E375A mutation was generated with QuikChange® II Site-Directed Mutagenesis kit.

pET15b-NSP13 WT	F	GGAATTCCATATGGAGAACCTGTACTTCCAAGGGGCTGTTGGGGCTTGTG
	R	CCGCTCGAGTTACAGATCCTCTTCAGAGATGAGTTTCTGCTCTTGTAAAGTTGCCACATTCCT
pET15b-NSP13 △stalk	F	GGTGGTGGTTCTGGTGGTGGTTCTATTGCTACTGTACGTGAAGTGC
	R	AGAACCACCACCAGAACCACCACCGCTACCAACACATGTA TTTTTATATA AAC
pET15b-NSP13 Z-linker-SH	F	GATAATGTTACTGACTTTAATGCAATT
	R	AGAACCACCACCAGAACCACCACCGCTACCAACACATGTA TTTTTATATA AAC
pET15b-NSP13 ZS-linker-H	F	GGTGGTGGTTCTGGTGGTGGTTCTATTGCTACTGTACGTGAAGTGC
	R	ACCATAAGAC AGTTTAAATG TCTCC
pET15b-NSP13 D374A/E375A ATPase mutant	F	AGCAGATATAGTTGTCTTTGCAGCAATTTCAATGGCCACAAATT
	R	AATTTGTGGCCATTGAAATTGCTGCAAAGACAACTATATCTGCT

2.2. Protein expression and purification

The recombinant SARS-CoV-2 NSP13 protein with C-terminal Myc tag was expressed in *Escherichia coli* (BL21 (DE3) PLySs, Transgene, China). BL21 (DE3) PLySs was cultured at 37 °C in Luria-Bertani medium containing ampicillin (100 μg/ml) until OD600 reached 0.6–0.8. Then, 0.5 mM isopropyl-b-d-thiogalactopyranoside (IPTG) was added to induce protein expression at 18 °C for 16 h–20 h. The collected bacteria were dissolved in lysis buffer (20 mM Tris-HCl pH7.4, 500 mM NaCl, 5% glycerol, 5 mM $MgCl_2$, 1 mM DTT, 0.01% Triton X-100, DNase I, RNase A, protease inhibitors) and disrupted by French pressure cell press under high pressure at 4 °C. The cell lysates were centrifuged at 18,000 rpm for 45min at 4 °C. The supernatant was incubated with Ni-NTA agarose beads (QIAGEN) at 4 °C for 4 h in the presence of 20 mM imidazole. After three times washing by wash buffer (20 mM Tris-HCl pH7.4, 500 mM NaCl, 5% glycerol, 4 mM $MgCl_2$, 1 mM DTT, 30 mM imidazole), proteins were eluted with elute buffer (20 mM Tris-HCl pH7.4, 500 mM NaCl, 5% glycerol, 4 mM $MgCl_2$, 1 mM DTT, 300 mM imidazole). The proteins were then purified by size-exclusion chromatography (Superdex200 10/300 GL, GE Healthcare) with SEC buffer (20 mM Tris-HCl pH7.4, 150 mM NaCl, 5% glycerol, 4 mM $MgCl_2$, 1 mM DTT). The proteins were concentrated using Amicon filter units Ultra-0.5 (30 kDa cutoff). Concentrated proteins were shock-frozen using liquid nitrogen and stored at −80 °C.

2.3. ATPase assay

We performed ATPase assay using a Quantichrom™ ATPase/GTPase assay kit (BioAssay Systems, USA). The ATPase activity was determined by detecting the release of free phosphate during ATP hydrolysis. 200 nM wild type or mutated proteins were incubated with various concentrations of ATP in buffer (20 mM Tris-HCl pH7.4, 40 mM NaCl, 4 mM $Mg(Ac)_2$, 0.5 mM EDTA) at 30 °C for 25min. Equal amount of SEC buffer was used as control. The ATP hydrolysis reaction was terminated by adding 200 μl Stop Reagent. After incubation for another 30min at room temperature, the absorbance was measured at 620 nm by a plate reader (Flexstation 3, Molecular Devices). The reaction velocity and ATP concentration were fitted to the Michaelis–Menten equation ($V=Vmax[S]/Km+[S]$).

2.4. Unwinding assay

The helicase activity of SARS-CoV-2 NSP13 was measured by FRET based unwinding assay. Two complementary single-strand RNAs (ssRNAs) were synthesized and labeled with Cy3 or BHQ2, respectively (Tsingke Biotechnology Co., Ltd.). ssRNA was dissolved in RNase free water. Complementary ssRNAs were denaturated at 95 °C for 5min followed by annealing through slowly cooling down to room temperature. For dsRNA unwinding, 5–10 nM purified proteins, 250 nM double-strand substrates and 2 μM competitor ssDNA, 2 mM ATP were diluted in reaction buffer (25 mM Hepes pH7.4, 40 mM KCl, 2 mM $MgCl_2$, 1 mM DTT, 0.01% Triton X-100) and the fluorescence of Cy3 was monitored by Flexstation 3 (Molecular Devices). The excitation light was set at 550 nm, the emission light was set at 620 nm, the cut off value was set at 610 nm, and the PMT sensitivity was set at low.

2.5. Biotin labeled 100 nt single-strand RNA in vitro transcription

A 100 nt ssRNA sequence (AGUAGCUGCACUUACUAACAAUGUUGCUUUUCAAACUGUCAAACCCGGUAAUUUUAACAAAGACUUCUAUGACUUUGCUGUGUCUAAGGGUUUCUUUAA) with less secondary structure was randomly selected from the NSP12 coding sequence of SARS-CoV-2. T7 RNA polymerase promoter sequence (GAAATTAATACGACTCACTATAGGG) was added to the 5' end of upstream primer. PCR products amplified from NSP12 coding sequence was used as transcription template. ssRNA was transcribed in vitro in the presence of Bio-16-UTP (AM8452, Invitrogen) using the HiScribe TM T7 Quick High Yield RNA Synthesis Kit (#E2050S, NEB), and further purified by RNA Clean XP (PN C63085AA, Beckman).

2.6. RNA pull down

20 μl Streptavidin Beads 6FF slurry (SA021005, SmartLifesciences) was added into 1.5 ml tube and washed three times with unwinding buffer (25 mM Hepes pH7.4, 40 mM KCl, 2 mM $MgCl_2$, 1 mM DTT, 0.01% Triton X-100). 350 μl of 2 μg/ml biotin labeled ssRNA was incubated with beads for 2 h at 4 °C. Remove the unbound ssRNA and wash the beads with unwinding buffer for three times. Then incubate beads with 500 nM proteins in unwinding buffer at 4 °C for 1 h. Wash the beads to remove unbound proteins, resuspend the beads with 30 μl 2 × SDS loading buffer and boil for 10min. The protein samples were analyzed by Western blot.

2.7. Thermal shift assay

The thermal stability of SARS-CoV-2 NSP13 was assessed using fluorescence-based thermal shift assay. 0.4 mg/ml proteins and SYPRO Orange fluorescent dye (Invitrogen) were incubated with or without 2 mM ATP. Samples were subjected to an increase in temperature from 25 °C to 90 °C in 0.5 °C increments per 20 s. Procedure was performed on a real time PCR machine. Fluorescence measurements were plotted and Tm values were calculated using GraphPad Prism.

2.8. Statistical analysis

The error bars in the figures represent the standard error of mean of three repeats or duplicates as indicated. The statistical significance of differences between groups was analyzed by *t*-test. $*P < 0.05$, $**P < 0.01$, $***P < 0.001$.

3. Results

3.1. The enzymatic activity of SARS-CoV-2 NSP13

We expressed SARS-CoV-2 NSP13 with an N-terminal 6 × His tag and C-terminal Myc tag in *Escherichia coli* and purified the proteins by Ni-NTA agarose beads and size-exclusion chromatography (Fig. 1A and B). We first examined the ATPase activity of SARS-CoV-2 NSP13. NSP13 exhibited ATPase activity in the absence of nucleic acids (Fig. 1C). When we mutated D374 and E375, which lie in the active pocket of the ATP binding site, to alanine (D374A/E375A) [23], NSP13 ATPase activity was dramatically impaired (Fig. 1C and D). We set up an in vitro dsRNA unwinding system based on FRET (fluorescence resonance energy transfer) [24] to evaluate the helicase activity of SARS-CoV-2 NSP13. A serial complementary ssRNA labeled with Cy3 or BHQ2 (Black Hole Quencher) was synthesized. When the complementary ssRNA was annealed to form an RNA duplex, Cy3 fluorescence was quenched by BHQ2 due to FRET. As the dsRNA is unwounded by the helicase, the quenching is alleviated (Fig. 1E). The data showed that SARS-CoV-2 NSP13 unwound dsRNA only when ATP was present (Fig. 1F). In addition, the D374A/E375A mutant showed little helicase activity, indicating that NSP13 helicase activity is dependent on ATP hydrolysis (Fig. 1G). The dsRNA unwinding activity of NSP13 was dose-dependent; as the concentration of NSP13 added increased, the unwinding rate increased (Fig. 1H and I). We also detected the processivity of NSP13 on dsRNA substrates with duplex regions of different lengths and found that unwinding of dsRNA decreased with increasing of duplex length, indicating that less unwinding events were complete for dsRNA substrates with longer duplex regions (Fig. 1J and Supplementary Table).

3.2. The stalk domain of NSP13 is essential for its helicase activity

As the role of the SARS-CoV-2 NSP13 stalk domain is not yet clear, we next explored whether the stalk domain is necessary for NSP13 activity. We constructed a NSP13 stalk deletion mutant (Δstalk) by replacing the stalk domain with a flexible linker (GGGS × 4) (Fig. 2A and B). We examined ATPase activity and found that NSP13 ATPase activity was disrupted when the stalk domain was deleted (Fig. 2C and D). Accordingly, deletion of the stalk domain abolished NSP13 helicase activity (Fig. 2E and F). These data demonstrated that the stalk domain is essential for the ATPase activity and helicase activity of NSP13, and that it functions as more than a linker connecting the ZBD and helicase domain.

3.3. The stalk domain mediated the rigid connection between the ZBD and helicase domain

SF1 helicases, such as Upf1 and NSP10 of EAV (equine arteritis virus), and NSP13 of MERS and SARS-CoV, share similar structural topologies [25]. Upf1, a eukaryotic RNA helicase, is the classical SF1 helicase [26]. The Upf1 CH domain (Cys/His rich domain, the counterpart of the NSP13 ZBD domain) may connect with the helicase domain through a flexible loop (invisible in electron density maps) and stalk domain (Fig. 3A) [27]. Compared to Upf1, the stalk domains of NSP13 of SARS-CoV-2 seem to provide relatively rigid connection between the ZBD and helicase domains (Fig. 3B). The stalk domains of NSP13 of SARS-CoV-2, SARS-CoV and MERS-CoV are highly conserved in sequence and structure (Fig. 3C and Fig. S1), and the stalk domain of NSP13 may affect its helicase activity through a tight interaction with the helicase domain.

Next, we sought to investigate whether the tight connection mediated by the stalk domain is needed for NSP13 function. To increase the flexibility between the ZBD and stalk domains or between the stalk and helicase domains of NSP13, we inserted a short flexible linker (GGGS × 2) between the ZBD and stalk domains (Z-linker-SH mutant) or between stalk and helicase domains (ZS-linker-H mutant) (Fig. 3D and E). We measured the ATP hydrolysis activity of these mutants. One mutant, ZS-linker-H, showed ATPase activity similar to that of WT NSP13. The other one, the Z-linker-SH mutant had slightly higher ATPase activity. These data indicated that increasing the flexibility between the ZBD and helicase domains by inserting a short flexible linker does not impair the ATPase activity of NSP13 (Fig. 3F and G). However, we found that the linker insertion at the two sites resulted in completely opposite effects on the dsRNA unwinding ability of NSP13. The unwinding activity of the Z-linker-SH mutant was not affected, whereas the ZS-linker-H mutant failed to unwind dsRNA (Fig. 3H and I). These findings implied that the rigid connection between the stalk and helicase domains is critical for the helicase activity without affecting the ATPase activity.

3.4. Linker insertion between the stalk and helicase domains interfered with the RNA binding of NSP13

The structure of NSP13 indicates that the stalk domain is located close to the RNA binding pocket, and it is predicted that the stalk domain might directly contribute to the interaction between NSP13 and RNA, although a structure of NSP13 and RNA in complex is lacking (Fig. S2) [15,28]. We examined the interaction of ssRNA with NSP13 by RNA pull down and found that linker insertion between the ZBD and stalk domains (Z-linker-SH) did not affect the RNA binding of NSP13, consistent with the unaffected RNA unwinding activity we showed above. In contrast, linker insertion between the stalk and helicase domains (ZS-linker-H) partially interfered with the binding of RNA to NSP13, indicating that the tight connection

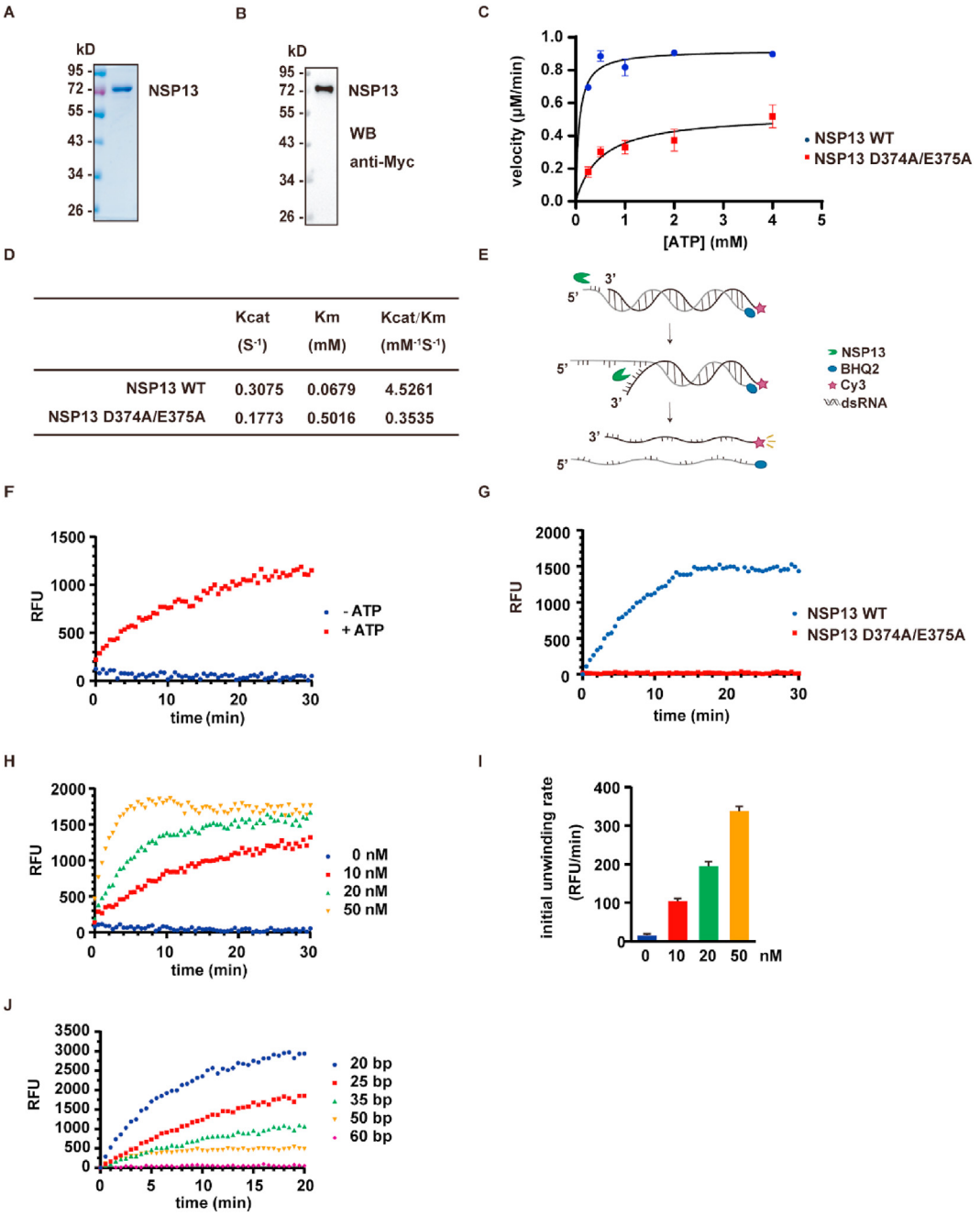

	Kcat (S^{-1})	Km (mM)	Kcat/Km ($mM^{-1}S^{-1}$)
NSP13 WT	0.3075	0.0679	4.5261
NSP13 D374A/E375A	0.1773	0.5016	0.3535

Fig. 1. NSP13 possesses ATP dependent dsRNA unwinding activity. A. Recombinant SARS-CoV-2 NSP13 protein purification. SDS-PAGE analysis of the purified NSP13 protein, and the gel was stained with Coomassie Blue. B. Western blot analysis of the purified NSP13 protein with anti-Myc antibody. C&D. ATPase activity of NSP13. (C) The ATPase activities of wild type (WT) and mutant (D374A/E375A) SARS-CoV-2 NSP13, the data were calculated by the Michaelis–Menten equation. (D) The Kcat, Km and Kcat/Km values of NSP13 WT and D374A/E375A mutant. E. Schematic illustration of the FRET-based dsRNA unwinding assay. Two complementary nucleic acid strands are labeled with Cy3 and the quencher BHQ2, respectively. The fluorescence of Cy3 is quenched by BHQ2 upon annealing of the RNA. With the unwinding of RNA duplexes by NSP13 protein, the fluorescence of Cy3 increases. F. The unwinding activity of SARS-CoV-2 NSP13 in the presence or absence of ATP. G. The unwinding assay of WT and mutant (D374A/E375A) NSP13.H&I. The unwinding rate increases with the increment of NSP13 concentration (0, 10, 20 and 50 nM). (H) Real-time dsRNA unwinding kinetics. (I) Initial unwinding rate of NSP13 at different concentrations. The initial unwinding rate was calculated by the kinetics in the first 5min. J. The unwinding activity of NSP13 upon dsRNA with different length of duplexes region (20, 25, 35, 50 and 60 bp). (For interpretation of the references to color in this figure legend, the reader is referred to the Web version of this article.)

between the stalk and helicase domains is important for the interaction between NSP13 and RNA (Fig. 4A and B).

3.5. Linker insertion between the stalk and helicase domains reduced the stability of NSP13

Finally, we explored the stability of WT and mutated NSP13 by a fluorescence-based thermal shift assay. ATP stabilized NSP13 as the Tm (melting temperature) of NPS13 increased (1.91 °C) when ATP was present (Fig. S3). However, linker insertion between the stalk and helicase domains (ZS-linker-H) resulted in a lower Tm in both the absence and presence of ATP (Fig. 4C–F), which suggested a lower stability of the ZS-linker-H mutant. The stability of the Z-linker-SH mutant was similar to that of WT NSP13 in the thermal shift assay, in agreement with the finding that its enzymatic activity was similar to that of WT NSP13. Thus, increasing the flexibility

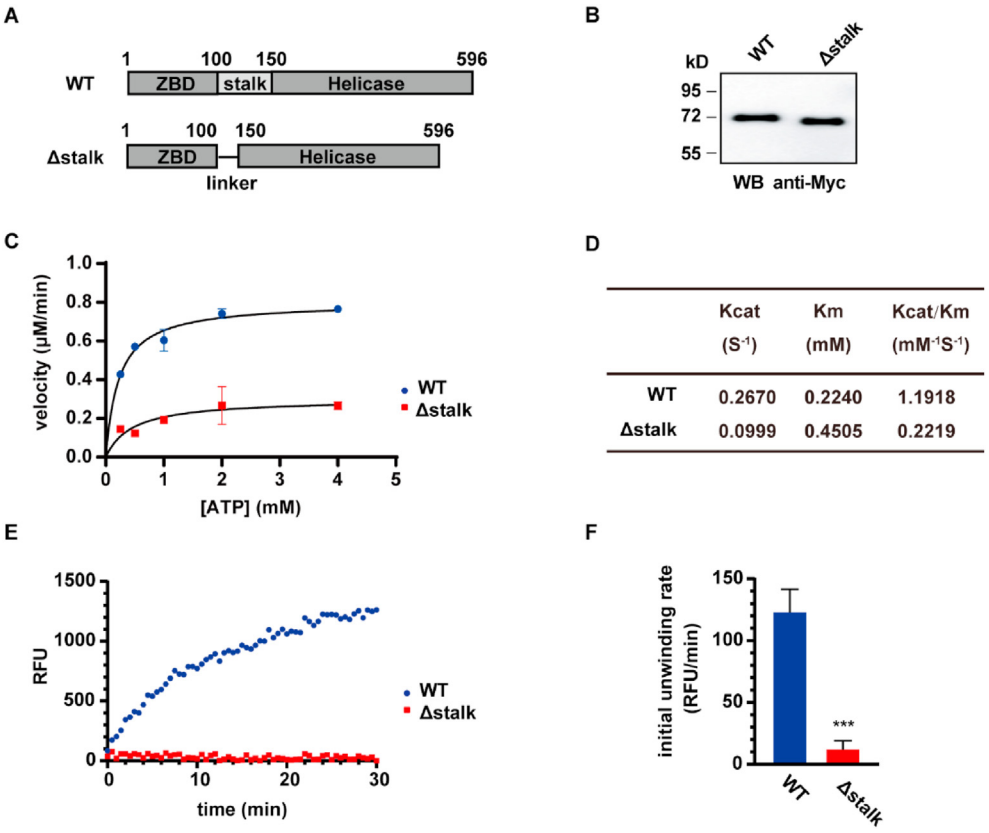

Fig. 2. The stalk domain plays a critical role in dsRNA unwinding by NSP13. A. Schematic illustration of WT NSP13 and Δstalk mutant. B. Western blot analysis of the purified WT and Δstalk mutant NSP13 proteins with anti-Myc antibody. C&D. Deletion of stalk domain abolished ATPase activity of SARS-CoV-2 NSP13. (C) ATPase activities of WT NSP13 and Δstalk mutant. (D) The Kcat, Km and Kcat/Km values of NSP13 WT and Δstalk mutant. E&F. Deletion of stalk domain disrupted dsRNA unwinding ability of NSP13. (E) The unwinding activity of WT NSP13 and Δstalk mutant. (F) The initial unwinding rate of WT NSP13 and Δstalk mutant. The initial unwinding rate was calculated by the kinetics in the first 5min. The significance was analyzed by *t*-test, ***$p < 0.001$.

between the stalk and helicase domains also reduces the protein stability of NSP13.

4. Discussion

SARS-CoV-2 NSP13 is an SF1 helicase [22]. Here we showed that SARS-CoV-2 NSP13 has ATPase activity in the absence of nucleic acids. It unwinds dsRNA in a manner dependent on ATP hydrolysis. The processivity of SARS-CoV-2 NSP13 in dsRNA unwinding seems better than that of the flavivirus NS3 helicase. It has been reported that the flavivirus NS3 helicase might dissociate every 18 bp in RNA unwinding, and it was not very efficient in duplex unwinding beyond 18bp in a bulk assay [29,30]. However, SARS-CoV-2 NSP13 could unwind dsRNA substrates with 35 bp or longer duplex regions, similar processivity was observed with SARS-CoV NSP13 [21]. As coronavirus has longest RNA genome (~30 kb) among RNA viruses, coronavirus helicases may also have better processivity in viral dsRNA unwinding during replication.

We verified the crucial role of the stalk domain in the enzymatic function of SARS-CoV-2 NSP13. We showed that deletion of the stalk domain impaired the ATPase activity of NSP13 and thus affected its helicase activity. Earlier studies demonstrated that several substitutions of Cys and His in the ZBD domain interfered with human coronavirus 229E NSP13 ATPase activity [31]. Although the ZBD and stalk domains are located far from the NSP13 ATP binding site and may not be directly involved in ATP hydrolysis, they may help to maintain the structure of the nearby helicase domain and facilitate the function of the helicase domain. Additional evidence indicated that the flexibility of the connections among the ZBD, stalk and helicase domains also affects NSP13 function. Insertion of the short flexible linker between the ZBD domain and stalk domain (Z-linker-SH) seemed to barely affect either the ATPase or helicase activity of NSP13, suggesting that a more flexible linkage between the ZBD and stalk domains is permissive. However, linker insertion between the stalk domain and helicase domain (ZS-linker-H) dramatically impaired NSP13 unwinding activity in an ATPase-independent manner, as its ATPase activity remained intact, implying that a rigid connection between the stalk domain and helicase domain is essential. According to the structure of NSP13, the stalk domain is predicted to located near the RNA binding pocket and may directly interact with the 3'end of RNA [15,28]. In addition, the stalk domain also affects NSP13 binding to RNA through its tight interaction with the Rec1A and Rec2A domains [15]. This was supported by the attenuated RNA binding ability of the ZS-linker-H mutant. Moreover, insertion of the short linker led to instability of NSP13, which also accounted for the compromised enzyme activity. These results suggest a tight structural and functional association between the stalk domain and helicase domain, suggesting the important role of the stalk domain in NSP13 activity.

NSP13 is conserved among beta-coronaviruses. There is only one different residue (I570 vs. V570) between NSP13 of SARS-CoV and NSP13 of SARS-CoV-2, and approximately 70% of the amino acids of NSP13 of SARS-CoV and MERS-CoV are identical [15,25]. This conservation suggests similarity in the enzymatic function of NSP13 among different coronaviruses. As an important component

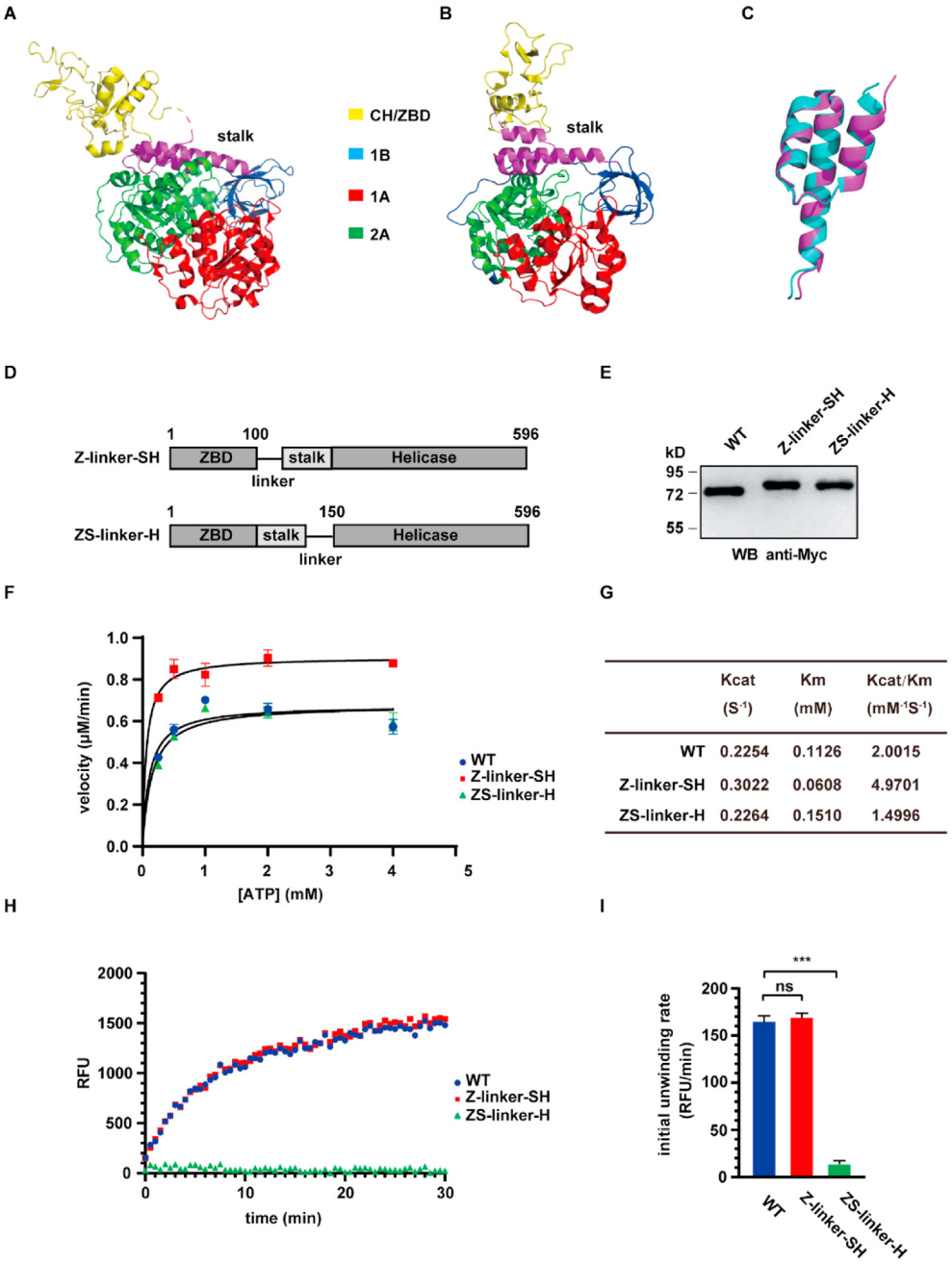

	Kcat (S^{-1})	Km (mM)	Kcat/Km ($mM^{-1}S^{-1}$)
WT	0.2254	0.1126	2.0015
Z-linker-SH	0.3022	0.0608	4.9701
ZS-linker-H	0.2264	0.1510	1.4996

Fig. 3. The rigid connection between stalk and helicase is essential to helicase activity but not ATPase activity. A&B. Overall structures of (A) Upf1 (PDB ID: 2wjy) and (B) SARS-CoV-2 NSP13 (PDB ID:6zsl) which were colored by different domains. The stalk domain was colored in magenta. C. Superimposition of NSP13 stalk domains from SARS-CoV-2 (magenta) and MERS-CoV (blue, PDB ID:5wwp). D. Schematic illustration of WT NSP13 and linker insertion mutants (Z-linker-SH and ZS-linker-H). E. Western blot analysis of the purified WT NSP13 and linker insertion mutants with anti-Myc antibody. F&G. Linker insertion did not affect ATPase activity of NSP13. (F) ATPase activity analysis of WT NSP13 and linker insertion mutants. (G) The Kcat, Km and Kcat/Km values of WT NSP13 and linker insertion mutants. H&I. Linker insertion between stalk and helicase domains abolished dsRNA unwinding activity of NSP13. (H) The unwinding assay of WT NSP13 and linker insertion mutants. (I) Initial unwinding rate of WT NSP13 and linker insertion mutants. The initial unwinding rate was calculated by kinetics in the first 5min. The significance was analyzed by *t*-test, ***$p < 0.001$. (For interpretation of the references to color in this figure legend, the reader is referred to the Web version of this article.)

of replication and transcription complex (RTC), NSP13 plays an important role in viral replication. Cryo-EM has solved the structure of the SARS-CoV-2 RTC, which comprises two NSP13 helicase proteins and one RNA polymerase NSP12 protein as well as one NSP7 and two NSP8 proteins, in complex with RNA [32,33]. In the complex structure, NSP13 did not directly interact with the RNA; therefore, no information about how RNA is unwound by the SARS-CoV-2 RTC could be obtained. Thus, although different models of dsRNA unwinding by NSP13 have been proposed based on the RTC structure [32,33], the detailed mechanism is still unclear. Further studies using an in vitro RNA unwinding assay with the RTC may provide more insights into SARS-CoV-2 replication.

Declaration of interests

The authors declare no competing interests.

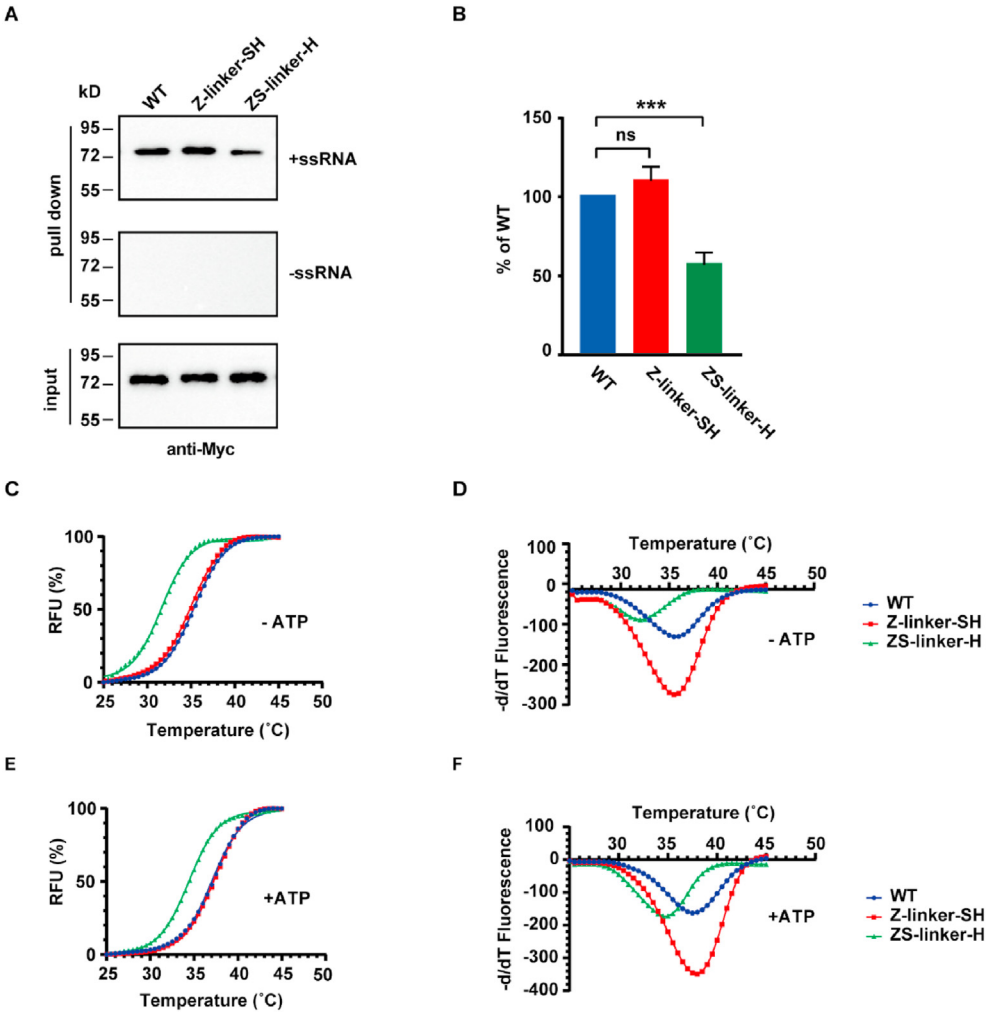

Fig. 4. Linker insertion between stalk and helicase domains affects the RNA binding and the stability of NSP13. A. RNA pull down assay to examine RNA binding of WT SARS-CoV-2 NSP13, and linker insertion mutants. B. Quantification of RNA binding ability of NSP13. The amount of WT NSP13 binding to RNA was set as 100%. The significance was analyzed by *t*-test, ***$p < 0.001$. C–F. Linker insertion between stalk and helicase domains affected the thermal stability of NSP13 in the absence or presence of ATP. (C&D) Thermal stability analysis of WT NSP13 and linker insertion mutants in the absence of ATP. (C) Fluorescence intensity of WT NSP13 and linker insertion mutants in the absence of ATP. (D) Melting curves of WT NSP13 and linker insertion mutants in the absence of ATP. In the absence of ATP, the melting temperature of WT NSP13, Z-linker-SH and ZS-linker-H were 35.33 °C, 34.97 °C and 31.61 °C, respectively. Compared with NSP13 WT, the melting temperature of Z-linker-SH showed a slight shift (−0.36 °C), while that of ZS-linker-H significantly decreased (−3.72 °C). (E&F) Thermal stability analysis of WT NSP13 and linker insertion mutants in the presence of ATP. (E) Fluorescence intensity of WT NSP13 and linker insertion mutants in the presence of ATP. (F) Melting curves of WT NSP13 and linker insertion mutants in the presence of ATP. In the presence of ATP, the melting temperature of WT NSP13, Z-linker-SH and ZS-linker-H were 37.24 °C, 37.36 °C and 34.38 °C, respectively. Compared with NSP13 WT, the melting temperature of Z-linker-SH showed no significant shift (+0.12 °C), while that of ZS-linker-H significantly decreased (−2.86 °C).

Acknowledgements.

We thank the funding from National Key R&D Program of China (2020YFA0707602), the National Natural Science Foundation of China (81622028), CAMS Innovation Fund for Medical Sciences (CIFMS) 2016-I2M-3-020 to support the project.

Appendix A. Supplementary data

Supplementary data to this article can be found online at https://doi.org/10.1016/j.bbrc.2022.02.068.

References

[1] S.S.A. Karim, Q.A. Karim, Omicron SARS-CoV-2 variant: a new chapter in the COVID-19 pandemic, Lancet 398 (2021) 2126–2128, https://doi.org/10.1016/S0140-6736(21)02758-6.

[2] E. Callaway, Delta coronavirus variant: scientists brace for impact, Nature 595 (2021) 17–18, https://doi.org/10.1038/d41586-021-01696-3.

[3] P. Zhou, X.L. Yang, X.G. Wang, B. Hu, L. Zhang, W. Zhang, H.R. Si, Y. Zhu, B. Li, C.L. Huang, H.D. Chen, J. Chen, Y. Luo, H. Guo, R.D. Jiang, M.Q. Liu, Y. Chen, X.R. Shen, X. Wang, X.S. Zheng, K. Zhao, Q.J. Chen, F. Deng, L.L. Liu, B. Yan, F.X. Zhan, Y.Y. Wang, G.F. Xiao, Z.L. Shi, A pneumonia outbreak associated with a new coronavirus of probable bat origin, Nature 579 (2020) 270–273, https://doi.org/10.1038/s41586-020-2012-7.

[4] F. Wu, S. Zhao, B. Yu, Y.M. Chen, W. Wang, Z.G. Song, Y. Hu, Z.W. Tao, J.H. Tian, Y.Y. Pei, M.L. Yuan, Y.L. Zhang, F.H. Dai, Y. Liu, Q.M. Wang, J.J. Zheng, L. Xu, E.C. Holmes, Y.Z. Zhang, A new coronavirus associated with human respiratory disease in China, Nature 579 (2020) 265–269, https://doi.org/10.1038/s41586-020-2008-3.

[5] V. Coronaviridae, Study Group of the International Committee on Taxonomy of, the species Severe acute respiratory syndrome-related coronavirus: classifying 2019-nCoV and naming it SARS-CoV-2, Nat. Microbiol. 5 (2020) 536–544, https://doi.org/10.1038/s41564-020-0695-z.

[6] C. Drosten, S. Gunther, W. Preiser, S. van der Werf, H.R. Brodt, S. Becker, H. Rabenau, M. Panning, L. Kolesnikova, R.A. Fouchier, A. Berger, A.M. Burguiere, J. Cinatl, M. Eickmann, N. Escriou, K. Grywna, S. Kramme, J.C. Manuguerra, S. Muller, V. Rickerts, M. Sturmer, S. Vieth, H.D. Klenk, A.D. Osterhaus, H. Schmitz, H.W. Doerr, Identification of a novel coronavirus in patients with severe acute respiratory syndrome, N. Engl. J. Med. 348 (2003) 1967–1976, https://doi.org/10.1056/NEJMoa030747.

[7] T.G. Ksiazek, D. Erdman, C.S. Goldsmith, S.R. Zaki, T. Peret, S. Emery, S. Tong, C. Urbani, J.A. Comer, W. Lim, P.E. Rollin, S.F. Dowell, A.E. Ling, C.D. Humphrey,

W.J. Shieh, J. Guarner, C.D. Paddock, P. Rota, B. Fields, J. DeRisi, J.Y. Yang, N. Cox, J.M. Hughes, J.W. LeDuc, W.J. Bellini, L.J. Anderson, S.W. Group, A novel coronavirus associated with severe acute respiratory syndrome, N. Engl. J. Med. 348 (2003) 1953–1966, https://doi.org/10.1056/NEJMoa030781.

[8] A.M. Zaki, S. van Boheemen, T.M. Bestebroer, A.D. Osterhaus, R.A. Fouchier, Isolation of a novel coronavirus from a man with pneumonia in Saudi Arabia, N. Engl. J. Med. 367 (2012) 1814–1820, https://doi.org/10.1056/NEJMoa1211721.

[9] A. Zumla, D.S. Hui, S. Perlman, Middle East respiratory syndrome, Lancet 386 (2015) 995–1007, https://doi.org/10.1016/S0140-6736(15)60454-8.

[10] S.R. Weiss, S. Navas-Martin, Coronavirus pathogenesis and the emerging pathogen severe acute respiratory syndrome coronavirus, Microbiol. Mol. Biol. Rev. 69 (2005) 635–664, https://doi.org/10.1128/MMBR.69.4.635-664.2005.

[11] S. Su, G. Wong, W. Shi, J. Liu, A.C.K. Lai, J. Zhou, W. Liu, Y. Bi, G.F. Gao, Epidemiology, genetic recombination, and pathogenesis of Coronaviruses, Trends Microbiol. 24 (2016) 490–502, https://doi.org/10.1016/j.tim.2016.03.003.

[12] A. Wu, Y. Peng, B. Huang, X. Ding, X. Wang, P. Niu, J. Meng, Z. Zhu, Z. Zhang, J. Wang, J. Sheng, L. Quan, Z. Xia, W. Tan, G. Cheng, T. Jiang, Genome Composition and divergence of the novel coronavirus (2019-nCoV) originating in China, Cell Host Microbe 27 (2020) 325–328, https://doi.org/10.1016/j.chom.2020.02.001.

[13] E.J. Snijder, E. Decroly, J. Ziebuhr, The nonstructural proteins directing coronavirus RNA Synthesis and processing, Adv. Virus Res. 96 (2016) 59–126, https://doi.org/10.1016/bs.aivir.2016.08.008.

[14] K.C. Lehmann, E.J. Snijder, C.C. Posthuma, A.E. Gorbalenya, What we know but do not understand about nidovirus helicases, Virus Res. 202 (2015) 12–32, https://doi.org/10.1016/j.virusres.2014.12.001.

[15] M.A. White, W. Lin, X. Cheng, Discovery of COVID-19 inhibitors targeting the SARS-CoV-2 Nsp13 helicase, J. Phys. Chem. Lett. 11 (2020) 9144–9151, https://doi.org/10.1021/acs.jpclett.0c02421.

[16] Z. Deng, K.C. Lehmann, X. Li, C. Feng, G. Wang, Q. Zhang, X. Qi, L. Yu, X. Zhang, W. Feng, W. Wu, P. Gong, Y. Tao, C.C. Posthuma, E.J. Snijder, A.E. Gorbalenya, Z. Chen, Structural basis for the regulatory function of a complex zinc-binding domain in a replicative arterivirus helicase resembling a nonsense-mediated mRNA decay helicase, Nucleic Acids Res. 42 (2014) 3464–3477, https://doi.org/10.1093/nar/gkt1310.

[17] M.E. Fairman-Williams, U.P. Guenther, E. Jankowsky, SF1 and SF2 helicases: family matters, Curr. Opin. Struct. Biol. 20 (2010) 313–324, https://doi.org/10.1016/j.sbi.2010.03.011.

[18] A.O. Adedeji, B. Marchand, A.J. Te Velthuis, E.J. Snijder, S. Weiss, R.L. Eoff, K. Singh, S.G. Sarafianos, Mechanism of nucleic acid unwinding by SARS-CoV helicase, PLoS One 7 (2012), e36521, https://doi.org/10.1371/journal.pone.0036521.

[19] K.A. Ivanov, V. Thiel, J.C. Dobbe, Y. van der Meer, E.J. Snijder, J. Ziebuhr, Multiple enzymatic activities associated with severe acute respiratory syndrome coronavirus helicase, J. Virol. 78 (2004) 5619–5632, https://doi.org/10.1128/JVI.78.11.5619-5632.2004.

[20] K.J. Mickolajczyk, P.M.M. Shelton, M. Grasso, X. Cao, S.E. Warrington, A. Aher, S. Liu, T.M. Kapoor, Force-dependent stimulation of RNA unwinding by SARS-CoV-2 nsp13 helicase, Biophys. J. 120 (2021) 1020–1030, https://doi.org/10.1016/j.bpj.2020.11.2276.

[21] N.R. Lee, H.M. Kwon, K. Park, S. Oh, Y.J. Jeong, D.E. Kim, Cooperative translocation enhances the unwinding of duplex DNA by SARS coronavirus helicase nsP13, Nucleic Acids Res. 38 (2010) 7626–7636, https://doi.org/10.1093/nar/gkq647.

[22] R. Weber, M. McCullagh, Role of ATP in the RNA translocation mechanism of SARS-CoV-2 NSP13 helicase, J. Phys. Chem. B 125 (2021) 8787–8796, https://doi.org/10.1021/acs.jpcb.1c04528.

[23] Z. Jia, L. Yan, Z. Ren, L. Wu, J. Wang, J. Guo, L. Zheng, Z. Ming, L. Zhang, Z. Lou, Z. Rao, Delicate structural coordination of the severe acute respiratory syndrome coronavirus Nsp13 upon ATP hydrolysis, Nucleic Acids Res. 47 (2019) 6538–6550, https://doi.org/10.1093/nar/gkz409.

[24] A.R. Ozes, K. Feoktistova, B.C. Avanzino, E.P. Baldwin, C.S. Fraser, Real-time fluorescence assays to monitor duplex unwinding and ATPase activities of helicases, Nat. Protoc. 9 (2014) 1645–1661, https://doi.org/10.1038/nprot.2014.112.

[25] W. Hao, J.A. Wojdyla, R. Zhao, R. Han, R. Das, I. Zlatev, M. Manoharan, M. Wang, S. Cui, Crystal structure of Middle East respiratory syndrome coronavirus helicase, PLoS Pathog. 13 (2017), e1006474, https://doi.org/10.1371/journal.ppat.1006474.

[26] S.E. Applequist, M. Selg, C. Raman, H.M. Jack, Cloning and characterization of HUPF1, a human homolog of the Saccharomyces cerevisiae nonsense mRNA-reducing UPF1 protein, Nucleic Acids Res. 25 (1997) 814–821, https://doi.org/10.1093/nar/25.4.814.

[27] M. Clerici, A. Mourao, I. Gutsche, N.H. Gehring, M.W. Hentze, A. Kulozik, J. Kadlec, M. Sattler, S. Cusack, Unusual bipartite mode of interaction between the nonsense-mediated decay factors, UPF1 and UPF2, EMBO J. 28 (2009) 2293–2306, https://doi.org/10.1038/emboj.2009.175.

[28] J.A. Newman, A. Douangamath, S. Yadzani, Y. Yosaatmadja, A. Aimon, J. Brandao-Neto, L. Dunnett, T. Gorrie-Stone, R. Skyner, D. Fearon, M. Schapira, F. von Delft, O. Gileadi, Structure, mechanism and crystallographic fragment screening of the SARS-CoV-2 NSP13 helicase, Nat. Commun. 12 (2021) 4848, https://doi.org/10.1038/s41467-021-25166-6.

[29] S. Xu, Y. Ci, L. Wang, Y. Yang, L. Zhang, C. Xu, C. Qin, L. Shi, Zika virus NS3 is a canonical RNA helicase stimulated by NS5 RNA polymerase, Nucleic Acids Res. 47 (2019) 8693–8707, https://doi.org/10.1093/nar/gkz650.

[30] S. Myong, M.M. Bruno, A.M. Pyle, T. Ha, Spring-loaded mechanism of DNA unwinding by hepatitis C virus NS3 helicase, Science 317 (2007) 513–516, https://doi.org/10.1126/science.1144130.

[31] A. Seybert, C.C. Posthuma, L.C. van Dinten, E.J. Snijder, A.E. Gorbalenya, J. Ziebuhr, A complex zinc finger controls the enzymatic activities of nidovirus helicases, J. Virol. 79 (2005) 696–704, https://doi.org/10.1128/JVI.79.2.696-704.2005.

[32] J. Chen, B. Malone, E. Llewellyn, M. Grasso, P.M.M. Shelton, P.D.B. Olinares, K. Maruthi, E.T. Eng, H. Vatandaslar, B.T. Chait, T.M. Kapoor, S.A. Darst, E.A. Campbell, Structural basis for helicase-polymerase coupling in the SARS-CoV-2 replication-transcription complex, Cell 182 (2020) 1560–1573, https://doi.org/10.1016/j.cell.2020.07.033, e1513.

[33] L. Yan, Y. Zhang, J. Ge, L. Zheng, Y. Gao, T. Wang, Z. Jia, H. Wang, Y. Huang, M. Li, Q. Wang, Z. Rao, Z. Lou, Architecture of a SARS-CoV-2 mini replication and transcription complex, Nat. Commun. 11 (2020) 5874, https://doi.org/10.1038/s41467-020-19770-1.